

Interband Four-Wave Mixing in Semiconductor Optical Amplifiers With ASE-Enhanced Gain Recovery

Prashant P. Baveja, *Student Member, IEEE*, Drew N. Maywar, *Member, IEEE*,
and Govind P. Agrawal, *Fellow, IEEE*

Abstract—We study, theoretically and experimentally, interband four-wave mixing in semiconductor optical amplifiers whose gain recovery is accelerated by amplified spontaneous emission (ASE). Across a broad range of wavelength shifts, we observe a considerable increase (over 20 dB) in the conversion efficiency, and a corresponding increase in the optical SNR (over 12 dB), as the device current is increased from 100 to 500 mA. For input pump powers below 1 mW, gain recovery in our device is dominated by internal ASE. Higher pump power levels reduce the conversion efficiency because of the pump-induced gain saturation near the output end. We show that wavelength shifts of up to 25 nm are possible, while maintaining a $>10\%$ conversion efficiency and a high optical SNR (>25 dB). A major advantage of our scheme is that the use of relatively low pump powers (<1 mW) reduces the electrical power consumption for such wavelength converters by more than a factor of 10. We discuss in detail the issue of optimum pump and signal powers. Our study is useful for realizing energy-efficient, modulation-format transparent, wavelength converters for optical networks.

Index Terms—Amplified spontaneous emission (ASE), four-wave mixing (FWM), gain-recovery time, semiconductor optical amplifiers (SOAs), wavelength conversion.

I. INTRODUCTION

FUTURE wavelength division multiplexing (WDM) networks are likely to employ phase modulation and polarization multiplexing; such networks will require fully transparent all-optical signal processing [1]–[6]. Four-wave mixing (FWM) is useful for wavelength conversion of WDM channels because it is transparent to the modulation format of the bit stream. Although FWM inside especially designed highly nonlinear fibers can be used for this purpose, the use of fibers requires high pump powers (>100 mW) in combination with a technique for suppressing stimulated Brillouin scattering [7]–[9]. With the recent

emphasis on low power consumption for modern telecommunication systems, the use of semiconductor optical amplifiers (SOAs) is desirable for making wavelength converters and other all-optical signal processing elements. SOAs are not only energy efficient but they can also amplify an optical signal while processing it.

FWM in SOAs has been studied and used for wavelength conversion for almost 25 years, and two mechanisms responsible for FWM in SOAs are known as *interband* and *intraband* FWM [10]. Interband FWM requires carrier-density modulation involving electron–hole recombination at relatively high frequencies and is typically limited by the carrier lifetime to small wavelength shifts of <0.1 nm [10], [11]. In contrast, intraband FWM involving modulation of occupational probability within an energy band can respond on a time scale of <1 ps and provides wavelength shifts larger than 10 nm [12]–[14]. For this reason, intraband FWM has been used for practical implementation of wavelength converters, even though required pump powers exceed 10 mW and the conversion efficiency is typically $<10\%$ [13]–[27].

The practical aspects of wavelength conversion for intraband FWM, such as the impact of input pump and signal powers on the conversion efficiency [13], [14], and the resulting optical signal-to-noise ratio (OSNR) of the converted signal [17], [18], have been investigated both theoretically and experimentally. Aside from high input pump powers and a poor conversion efficiency, such wavelength converters also operate over a limited range of signal powers, mainly because of slow gain recovery in the SOAs [17]. An optical beam at a wavelength near the transparency point of the SOA (called the assist or holding beam) with powers in excess of 40 mW has been used to reduce the SOA gain-recovery time to as low as 60 ps [28] and to enhance the performance of SOA-based wavelength converters [23]–[25].

Recently, commercial SOAs have become available whose gain-recovery time can be reduced to close to 10 ps at high drive currents [29]–[34]. The physical mechanism behind fast gain recovery is related to saturation of the SOA gain at high drive currents through amplified spontaneous emission (ASE), together with a reduced saturation energy realized by suitable doping of quantum wells. Such a small value of the gain-recovery time implies that these SOAs should exhibit interband FWM with wavelength shifts >10 nm, provided that the pump does not become intense enough to saturate the gain along the SOA length. Efficient FWM at high drive currents was first reported in 1997 in a 1.5-mm-long SOA [35]. More recently, SOAs with ASE-enhanced gain recovery were used to observe [36]

Manuscript received November 8, 2010; revised February 25, 2011; accepted March 17, 2011. Date of publication June 7, 2011; date of current version March 2, 2012. This work was supported in part by the National Science Foundation through the Award ECCS-1041982.

P. P. Baveja and G. P. Agrawal are with the Institute of Optics, University of Rochester, Rochester, NY 14627 USA (e-mail: baveja@optics.rochester.edu; gpa@optics.rochester.edu).

D. N. Maywar is with the Electrical, Computer, and Telecommunications Engineering Technology Department, Rochester Institute of Technology, Rochester, NY 14623 USA (e-mail: dnmiee@rit.edu).

Color versions of one or more of the figures in this paper are available online at <http://ieeexplore.ieee.org>.

Digital Object Identifier 10.1109/JSTQE.2011.2136372

efficient FWM at small pump–signal detunings (0.02 nm or less). Simultaneous wavelength conversion of two data channels has also been reported in a 2010 study [1].

In this paper, we carry out a detailed theoretical analysis of interband FWM in the presence of internal ASE and supplement it with experimental results designed to optimize the device performance for wavelength conversion. In Section II, we extend the theoretical model of interband FWM developed in 1988 [10] by incorporating the effects of ASE-induced gain saturation and use it to predict numerically how the conversion efficiency changes as a function of pump–signal detuning, SOA current, pump power, and the effective carrier lifetime. Section III describes our experimental setup and focuses on the results showing the impact of increasing the SOA current and pump–signal detuning on the FWM process. We use the conversion efficiency and the idler OSNR as the two figures of merit for characterizing the FWM process. In section IV, we discuss the role of input pump and signal powers for optimizing the conversion efficiency and OSNR of a wavelength converter. We also discuss the feasibility of all-optical regeneration using FWM at high drive currents. We compare the theory and experiments in Section V and summarize the main results in Section VI.

II. THEORETICAL MODEL WITH ASE EFFECTS

To study interband FWM in the presence of ASE, we adopt a model developed in [10]. We assume that the pump, signal, and idler fields propagate as transverse electric (TE) modes of the SOA and they remain linearly polarized. The FWM problem can then be studied by solving the scalar wave equation

$$\nabla^2 E - \frac{n^2}{c^2} \frac{\partial^2 E}{\partial t^2} = \frac{1}{\epsilon_0 c^2} \frac{\partial^2 P}{\partial t^2} \quad (1)$$

where n is the refractive index, ϵ_0 is the permittivity in free space, and c is the speed of light in vacuum. The total electric field E inside the amplifier has the form

$$E(x, y, z, t) = U(x, y)A(z, t) \exp(i\beta_0 z - i\omega_0 t) \quad (2)$$

where $U(x, y)$ is the mode profile and $A(z, t)$ is the slowly varying part of the field. The propagation constant β_0 is related to the pump frequency ω_0 by the usual relation $\beta_0 = \bar{n}\omega_0/c$, where \bar{n} is the mode index.

The induced polarization can be related to the SOA gain g using $P = \epsilon_0 \chi E$, where $\chi = (\alpha + i)gc/\omega_0$ is the susceptibility and α is the linewidth enhancement factor responsible for changes in the mode index [10]. Using this form and the slowly varying envelope approximation, the evolution of $A(z, t)$ inside the SOA is governed by

$$\frac{\partial A}{\partial z} + \frac{1}{v_g} \frac{\partial A}{\partial t} = \frac{g}{2}(1 - i\alpha)A(z, t) \quad (3)$$

where v_g is the group velocity.

The SOA gain g depends on the carrier density N inside the active region as $g(z, t) = \Gamma a(N - N_0)$, where Γ is the mode confinement factor, a is a material parameter (referred to as the gain cross section), and N_0 is the value of carrier density at which the SOA becomes transparent. The carrier density is

found by solving the rate equation [37]

$$\frac{\partial N}{\partial t} = \frac{I}{qV} - \frac{N}{\tau_c} - \frac{g(N)}{\hbar\omega_0} |A|^2 \quad (4)$$

where I is the current injected into the SOA and V is the volume of the active region. The carrier lifetime τ_c itself depends on N . Including both the radiative and nonradiative recombination processes, it can be written in the form [37]

$$\tau_c(N) = [A_{nr} + B_{sp}N + C_a N^2]^{-1} \quad (5)$$

where A_{nr} , B_{sp} , and C_a are three constants whose values depend on the SOA design. Equation (4) can be used to obtain the following equation for the optical gain [10]:

$$\frac{\partial g}{\partial t} = \frac{g_0 - g}{\tau_c} - \frac{g|A|^2}{E_{\text{sat}}} \quad (6)$$

where $E_{\text{sat}} = \hbar\omega_0\sigma/a$ is the saturation energy, σ is the mode area, and the unsaturated gain g_0 depends on the injected current I as

$$g_0(I) = \Gamma a N_0 (I/I_0 - 1) \quad (7)$$

where $I_0 = qVN_0/\tau_{c0}$ is the current required for transparency and τ_{c0} is the carrier lifetime at $N = N_0$.

In our SOAs, the effects of ASE should be incorporated in the gain equation. Although a complete model should consider amplification of spontaneous emission in both the forward and backward directions over the entire SOA gain bandwidth [38], here we adopt a simple model discussed in [34] and replace $|A|^2$ in (6) with $|A|^2 + P_{\text{ASE}}$, where P_{ASE} is the total ASE power. The resulting modified gain equation can be written in the form

$$\frac{\partial g}{\partial t} = \frac{g_0}{\tau_c} - \frac{g}{\tau_{\text{eff}}} - \frac{g|A|^2}{E_{\text{sat}}} \quad (8)$$

where the effective gain-recovery time is defined as

$$\frac{1}{\tau_{\text{eff}}} = \frac{1}{\tau_c} + \frac{P_{\text{ASE}}}{E_{\text{sat}}} = \frac{1}{\tau_c} + \frac{1}{\tau_{\text{ASE}}} \quad (9)$$

The origin of interband FWM lies in the gain-saturation term in (6). More specifically, when a signal field at frequency ω_1 is launched together with the pump, the amplitude A contains three terms

$$A = A_0 + A_1 \exp(-i\Omega t) + A_2 \exp(i\Omega t) \quad (10)$$

where the subscripts 0, 1, and 2 stand for the pump, signal, and idler fields, respectively, and $\Omega = \omega_1 - \omega_0$ represents pump–signal detuning. The idler frequency $\omega_2 = \omega_0 - \Omega$ is generated such that the FWM condition $2\omega_0 = \omega_1 + \omega_2$ is automatically satisfied. Because the total intensity $|A|^2$ contains terms oscillating at the beat frequency Ω , the gain is also modulated at this frequency, and the modified gain equation (8) has an approximate solution of the form

$$g = \bar{g} + [\Delta g \exp(-i\Omega t) + c.c.] \quad (11)$$

where the average gain \bar{g} is given by

$$\bar{g} = \frac{g_0}{r + (|A_0|^2 + |A_1|^2 + |A_2|^2)/P_{\text{sat}}} \quad (12)$$

and the amplitude Δg of gain modulations created by the beating of the pump with the signal is given by

$$\Delta g = -\frac{\bar{g}(A_1 A_0^* + A_0 A_2^*)}{P_{\text{sat}}(r - i\Omega\tau_c)}. \quad (13)$$

In writing the preceding solution for the gain, we have introduced two parameters defined as

$$r = \tau_c / \tau_{\text{eff}}, \quad P_{\text{sat}} = E_{\text{sat}} / \tau_c. \quad (14)$$

The dimensionless parameter $r \geq 1$ represents the factor by which the gain-recovery time is reduced by the ASE-induced gain saturation. For $r = 1$, (12) and (13) reduce to the standard solution for carrier density pulsations discussed in [10] in the absence of ASE. It can be seen from (12) that as the gain-recovery time is shortened, the small-signal gain g_0 is reduced by a factor of r because of gain saturation induced by ASE [34]. Fortunately, this reduction is accompanied with a considerable enhancement of the bandwidth over which gain modulations can occur. This is apparent from the presence of the factor r in (13) and is the origin of large wavelength shifts realized in such SOAs through interband FWM.

The final step is to use (10) and (11) in (3) and separate the oscillating and nonoscillating terms. In the continuous wave (CW) case studied here, we can drop the time derivative in (3). We then obtain the following three coupled differential equations for the pump, signal, and idler fields:

$$2\frac{dA_0}{dz} = (1 + i\alpha)[\bar{g}A_0 + (\Delta g A_2 + \Delta g^* A_1)] \quad (15)$$

$$2\frac{dA_1}{dz} = (1 + i\alpha)(\bar{g}A_1 + \Delta g A_0) \quad (16)$$

$$2\frac{dA_2}{dz} = (1 + i\alpha)(\bar{g}A_2 + \Delta g^* A_0). \quad (17)$$

Equations (15)–(17) can be solved analytically in the undepleted pump approximation [14]. However, since the pump is amplified considerably inside our SOAs operated at high currents, this approximation is not valid near the output end. For this reason, we solve the three coupled equations numerically and include all pump-depletion effects. To improve the numerical accuracy, we allow saturation of the average gain \bar{g} in (12) by all three optical fields. However, we assume that the wavelength dependence of the gain and the α factor is negligible over the pump–signal detuning range of interest (about 10 nm). These assumptions are reasonable for most SOAs [39], [40].

The conversion efficiency and the OSNR are two critical figures of merit for FWM-based wavelength converters [4], [17], [21]. We define them as

$$\eta = P_2(L)/P_1(0), \quad \text{OSNR} = P_2(L)/P_n \quad (18)$$

where L is the SOA length, $P_1 = |A_1(0)|^2$ is the input signal power, and $P_2 = |A_2(L)|^2$ is the output idler power. The noise power P_n used to define the OSNR is obtained by using $P_n = p_n N_{\text{BW}}$, where p_n is the noise spectral density and N_{BW} is the reference bandwidth. For telecommunication signals, OSNR is commonly defined over a 0.1-nm noise bandwidth [21], [41]. However, our experiments are performed with CW signals. Therefore, for the sake of consistency, we assume

TABLE I
PARAMETER VALUES USED IN NUMERICAL SIMULATIONS

Parameter	Symbol	Value
Device length	L	1 mm
Gain cross section	a	$10.2 \times 10^{-20} \text{ m}^2$
Linewidth enhancement factor	α	3
Mode-confinement factor	Γ	0.47
Current at transparency	I_0	47.5 mA
Carrier density at transparency	N_0	$2.7 \times 10^{23} \text{ m}^{-3}$
Carrier lifetime at transparency	τ_c	200 ps
Nonradiative recombination rate	A_{nr}	$4.3 \times 10^9 \text{ s}^{-1}$
Spontaneous recombination rate	B_{sp}	$4.7 \times 10^{-16} \text{ m}^3/\text{s}$
Auger recombination coefficient	C_a	$2.0 \times 10^{-40} \text{ m}^6/\text{s}$
Saturation energy	E_{sat}	0.7 pJ

that our input signal power represents the average power of a WDM channel containing return-to-zero Gaussian pulses with a 50% duty cycle.

The numerical results presented in this section focus on calculating the conversion efficiency η , using the device and input parameters listed in Table I for a commercial SOA (CIP Technologies, model SOA-XN-OEC-1550) designed for high internal ASE at high drive currents. Using the procedure outlined in [34], we estimate some device parameters from the experimental measurements of the SOA gain (under low input power conditions) as a function of drive current. One such parameter is the ASE power P_{ASE} , assumed to be constant all along the SOA length. We calculate the ASE power by using the relation $P_{\text{ASE}} = DN^2$ with $D = 1.32 \times 10^{-50} \text{ m}^6 \text{ W}$, a value deduced based on our experimental measurements in [34].

Fig. 1(a) shows changes in η as a function of pump–signal detuning [$\Delta\lambda = (\lambda_0^2/2\pi c)\Omega$] at three different drive currents for fixed input pump and signal powers (0 and $-25 \text{ dB}\cdot\text{m}$, respectively). As expected, η decreases rapidly with $\Delta\lambda$ at any drive current. However, η increases by more than 20 dB, at any pump–signal detuning, as the drive current is increased from 100 to 500 mA. This enhancement of conversion efficiency is due to the ASE-induced shortening of the gain-recovery time. From a practical standpoint, the important question is how large is the $\Delta\lambda$ range over which the interband FWM can provide wavelength conversion with a net gain ($\eta > 0 \text{ dB}$). This range is only 0.3 nm at 100 mA but it increases to almost 7.5 nm at 500 mA. Noting that the wavelength shift is $2\Delta\lambda$, the model predicts that our SOA can provide wavelength shifts of up to 15 nm when driven at high current levels. Physical mechanism for the large improvement is a reduction of the gain-recovery time at high currents (or high ASE levels). If we are willing to accept a 10% conversion efficiency, wavelength shifts can exceed 25 nm. It is remarkable that this kind of performance can be realized at a relatively low 1-mW pump power.

One may wonder whether higher pump powers would make the situation even better because pump powers $>10 \text{ mW}$ are routinely used in the case of intraband FWM [4], [26], [27]. It is therefore important to see the effect of input P_0 on interband FWM. In Fig. 1(b), we plot η as a function of $\Delta\lambda$ for three input pump powers while keeping the SOA drive current fixed

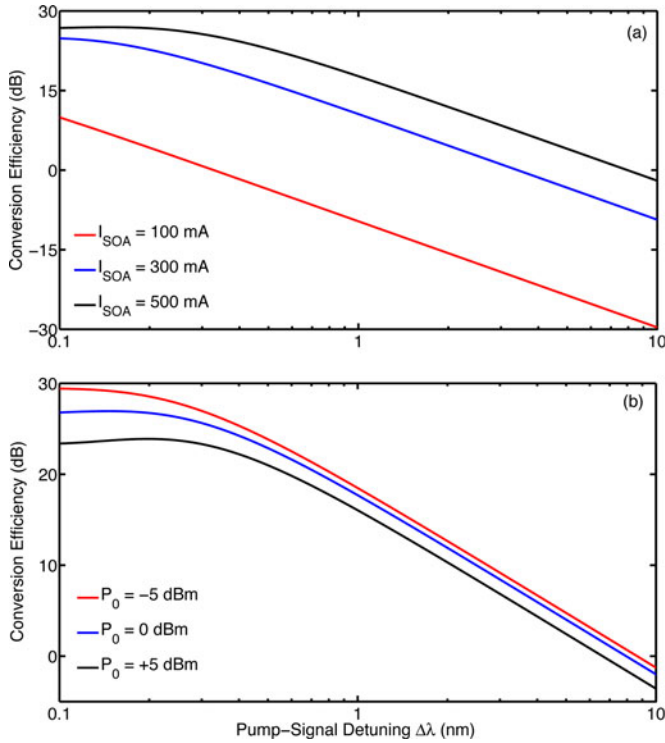


Fig. 1. Conversion Efficiency as a function of pump-signal detuning (a) at three drive currents for 1 mW pump power and (b) at three input pump powers at 500-mA drive current.

at 500 mA and input signal power at -25 dB-m. As the pump power increases, the conversion efficiency at any $\Delta\lambda$ is actually reduced. This is somewhat counterintuitive but can be understood by noting that, if the gain is saturated considerably by the pump, the impact of ASE is reduced. Physically speaking, as the pump is amplified by the SOA, its power increases and becomes comparable to the ASE power near the output SOA end. Gain saturation by such an intense pump decreases the ASE power, which increases the gain-recovery time and reduces the conversion efficiency. This is the reason why higher input pump powers should be avoided for wavelength converters making use of ASE-induced gain saturation. This is not a limitation because the use of low pump powers is desirable from the standpoint of low electrical power consumption for telecommunication applications. Fig. 1(b) shows that the pump power should be kept below 1 mW to avoid pump-induced gain saturation. We discuss experimental optimization of pump and signal powers in Section IV.

To establish that the conversion efficiency is indeed enhanced by the ASE-induced shortening of the gain-recovery time, we study changes in the η as a function of τ_{eff} . We assume that the SOA has a carrier lifetime of 1000 ps and is biased to provide a gain of 30 dB, both in the presence and absence of internal ASE ($g_0L = 6.908$). Fig. 2 shows η calculated numerically as a function of τ_{eff} for three values of $\Delta\lambda$. In all three cases, η improves dramatically as τ_{eff} becomes shorter. For a relatively small detuning ($\Delta\lambda = 0.1$ nm), a net idler gain can be obtained for $\tau_{\text{eff}} < 300$ ps. This is consistent with the earlier results on nearly degenerate FWM [10], [14]. However, for a large 10-nm

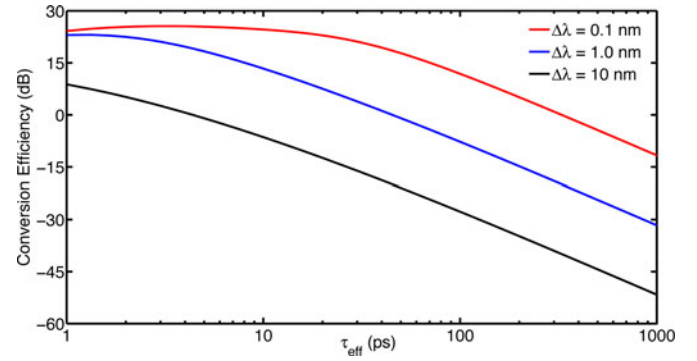


Fig. 2. Conversion Efficiency as a function of effective carrier lifetime τ_{eff} for different pump-signal detuning $\Delta\lambda$. Device gain $G_0 = 30$ dB

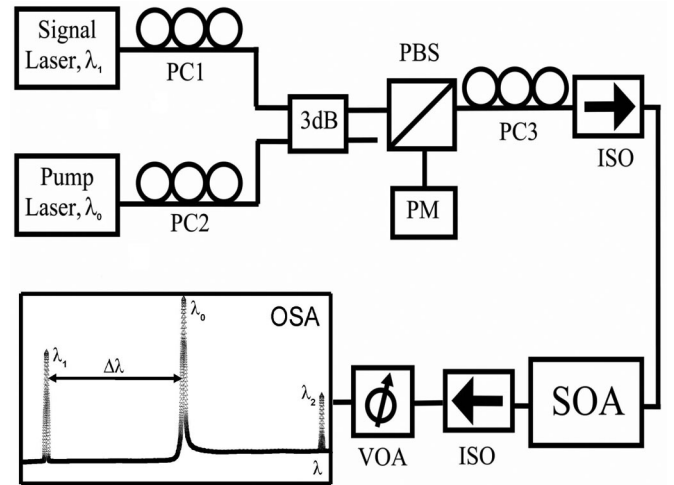


Fig. 3. Experimental setup used for studying interband FWM. PC: polarization controller; PBS: polarization beam splitter; PM: power meter; VOA: variable optical attenuator; ISO: isolator; OSA: optical spectrum analyzer; $\Delta\lambda$: pump-signal detuning.

detuning, η is below -30 dB if τ_{eff} exceeds 100 ps. This is the reason why interband FWM was not found to be suitable for wavelength conversion. However, if τ_{eff} can be reduced to below 10 ps, $\eta > 1$ can be realized even for $\Delta\lambda = 10$ nm. These results clearly show how the ASE-induced shortening of τ_{eff} can extend the usefulness of interband FWM for wavelength conversion.

III. DEVICE CHARACTERIZATION AND FWM RESULTS

In Section II, we established theoretically that interband FWM can be used for wavelength conversion over a large range using low input pump powers if SOAs with a short gain-recovery time are employed. To verify our theoretical predictions and to investigate various tradeoffs required for wavelength-conversion performance optimization, we perform a series of experiments using the setup shown in Fig. 3.

In our setup, the pump and signal are combined using a 3-dB coupler and sent through a polarization beam splitter (PBS) whose role is to ensure that pump and signal remain copolarized throughout the experiment and excite only the TE mode of the SOA. The pump wavelength λ_0 is fixed at 1574.93 nm to keep it close to the SOA gain peak at 1570 nm. The signal wavelength

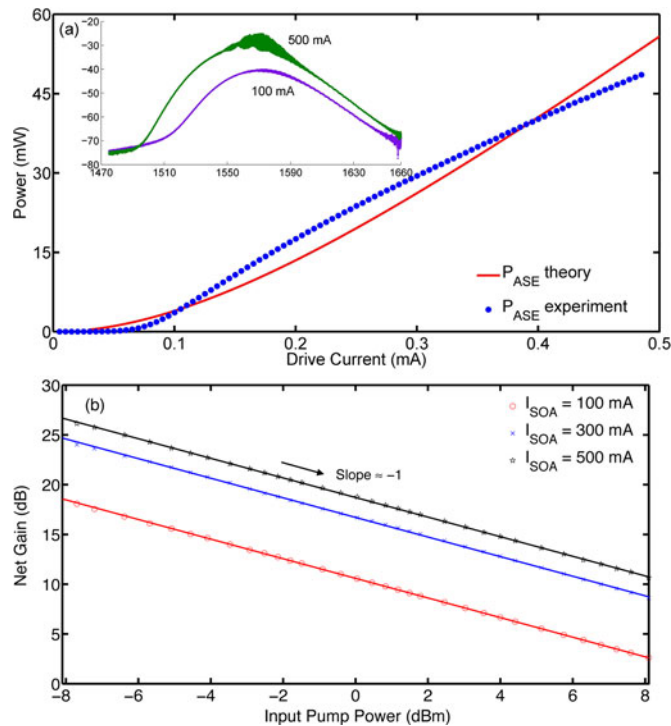


Fig. 4. (a) Measured (circles) and calculated (solid line) ASE power as a function of drive current. The inset shows the ASE spectra at 100 and 500 mA. (b) Net device gain as a function of pump power. Input signal power and pump-signal detuning $\Delta\lambda$ were -20.3 dB·m and 2.5 nm, respectively.

λ_1 is tuned over a wide range on the short-wavelength side (blue-shifted). The insertion and coupling losses after the PBS are estimated to be 3 dB. The isolators are used to minimize back reflections. A variable optical attenuator (Agilent 8156A) was used at the SOA output to ensure that optical powers at the optical spectrum analyzer were below its safe limit. It was calibrated using a broad-band ASE source and exhibited a 3.3-dB insertion loss, while providing 20-dB attenuation over 1500–1600 nm with a wavelength dependence of <0.2 dB. The total attenuation at the output end, including output coupling loss and insertion losses of the isolator and optical attenuator, was estimated to be 30.3 dB at 1570 nm; its wavelength dependence was negligible in the wavelength range 1565–1585 nm. The SOA temperature was fixed at 25 °C for all the measurements.

Before reporting our FWM results, we discuss the measurements performed to characterize the SOA. Fig. 4(a) shows both the calculated and measured ASE power (over the entire ASE bandwidth) as a function of the drive current [34]. The ASE power increases drastically as I_{SOA} is increased from 100 to 500 mA, becoming close to 50 mW at 500 mA and reducing the gain-recovery time from 100 to 10 ps. The inset shows the ASE spectra at 100 and 500 mA bias currents. The gain peak of the spectrum near 1570 nm shifts toward the blue side with increasing current. However, we also see a considerable increase in the amplitude of rapid oscillations near the gain peak at high drive currents. These oscillations have a period of 0.3 nm and have their origin in the residual feedback at the two SOA facets, resulting in Fabry–Perot effects [42]. As discussed in Section V,

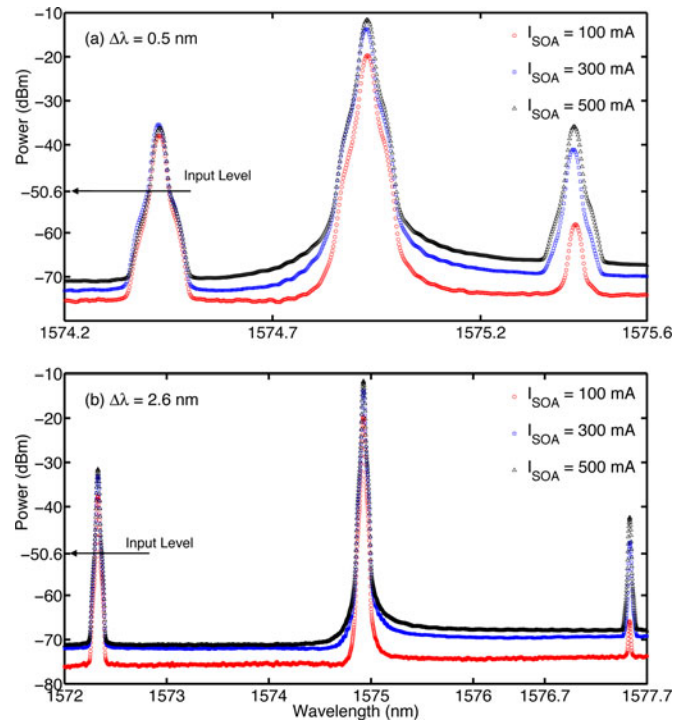


Fig. 5. FWM spectra measured at three currents for a pump-signal detuning of (a) 0.5 nm and (b) 2.6 nm at a pump power of -3.3 dB·m. The input signal level (-20.3 dB·m) is marked by an arrow.

they constitute a major source of mismatch between our theoretical predictions and experimental results.

In Fig. 4(b), we plot the net SOA gain as a function of input pump power at three drive currents. The net gain is defined as the ratio of total output power (sum of pump, signal, and idler powers) to total input power (sum of pump and signal power). The solid lines in Fig. 4(b) represent a linear fit to the experimental data. A negative slope of -1 is expected from the saturation of average gain in (12). A different slope would indicate the onset of intraband effects [42] and is observed in traditional SOAs [16]. These results confirm that the intraband FWM effects are almost negligible in the range of input pump powers used in our experiments.

We next study the impact of increasing the drive current I_{SOA} on the FWM process. Fig. 5 shows the optical spectra at the SOA output for two different pump-signal detunings. The peak on the right side of the pump corresponds to the idler created through interband FWM. For $\Delta\lambda = 0.5$ nm, the idler is generated at current levels as low as 100 mA, and its power increases by more than 20 dB as I_{SOA} is increased to 500 mA. Multiple signal-idler pairs are observed with increasing I_{SOA} (not shown here) in agreement with previously reported results for small $\Delta\lambda$ [36].

At a large pump-signal detuning of 2.6 nm, negligible FWM occurs at low drive currents (<120 mA). However, the idler is greatly enhanced with increasing I_{SOA} , indicating a sharp reduction in the gain-recovery time induced by the enhanced ASE [31]–[34], [36]. From our theory of Section II, the magnitude of idler peak corresponds to an effective carrier lifetime of 21 and 10 ps at 300 and 500 mA, respectively (calculated using the method outlined in [34]).

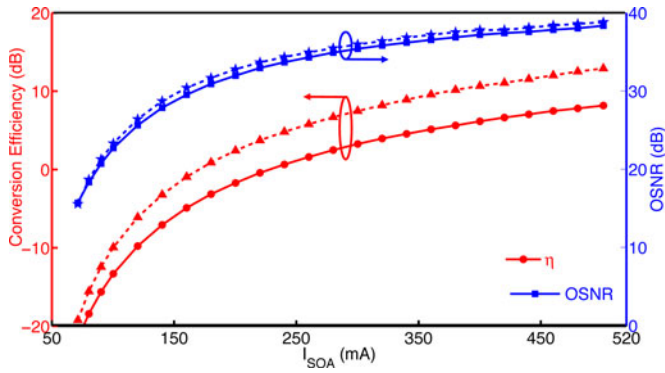


Fig. 6. Conversion efficiency and OSNR as a function of I_{SOA} for $\Delta\lambda = 0.5$ nm at a pump power of -3.3 dB-m (dashed curves) and $+3.3$ dB-m (solid curves). Input signal power was -10 dB-m.

The FWM spectra in Fig. 5 show that the ASE-noise spectral density near the idler wavelength increases by more than 7 dB as I_{SOA} is increased from 100 to 500 mA. Since the ASE power is increasing, we need to ensure that the improvement in the conversion efficiency η at large I_{SOA} is not accompanied with a degradation of the OSNR at the converted wavelength. To understand this issue, we plot in Fig. 6, η and OSNR as a function of drive current for two different pump powers. As seen there, OSNR actually increases with increasing current, indicating that the increase in the in-band ASE noise is more than compensated by the considerable increase in the idler power. An OSNR of > 30 dB along with a reasonable conversion efficiency ($\eta > 50\%$) can be achieved for $I_{SOA} > 160$ mA. At a pump power of $+3.3$ dB-m, η decreases by about 4 dB because of pump-induced gain saturation (discussed in Section II), but the corresponding reduction in OSNR is much smaller (< 0.5 dB). This can be explained by noting that, while the idler power is reduced considerably at higher pump powers, the in-band ASE noise is also reduced because of pump-induced gain saturation.

From a practical standpoint, the relevant issue is how large wavelength shifts are possible if such SOAs are used as wavelength converters, or how large $\Delta\lambda$ can be while maintaining good conversion efficiency and OSNR. Fig. 7 shows the conversion efficiency η and OSNR as a function of $\Delta\lambda$ at the same two pump powers. As expected, both degrade as $\Delta\lambda$ increases, indicating that one should not increase $\Delta\lambda$ beyond an upper limit. If we use $\eta > -10$ dB (10%), as an acceptance criterion, this upper limit is < 1 nm at 100 mA but increases to more than 10 nm at 500 mA. At any detuning, η and OSNR are enhanced by more than 20 and 12 dB, respectively, when drive current is increased from 100 to 500 mA. This increase in η and OSNR is observed for both pump powers.

As we saw in Section II, the enhancement in η is due to faster gain recovery caused by a large increase in the ASE power at high currents [31]–[34], [36]. Enhancement in η (or the idler power) with increasing drive current does not translate entirely to an increase of OSNR. In Fig. 7, a 20-dB enhancement in η translates into an OSNR increase of only about 12 dB as current is increased from 100 to 500 mA. However, the OSNR exceeds 20 dB up to a detuning of about 5 nm at -3.3 dB-m pump power at a drive current of 500 mA. With an increase in input pump

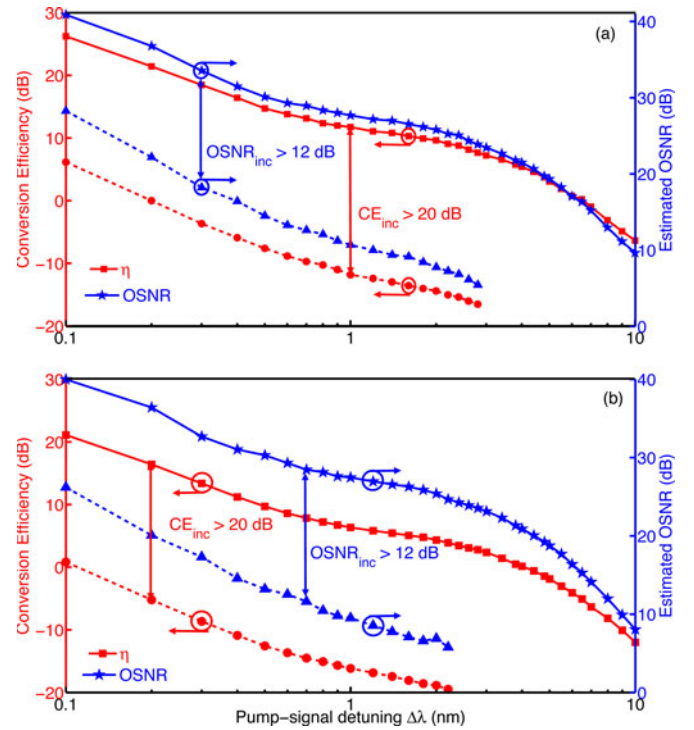


Fig. 7. Conversion efficiency and OSNR as a function of $\Delta\lambda$ at a pump power of (a) -3.3 dB-m and (b) $+3.3$ dB-m for input signal power of -20.3 dB-m. Dashed and solid curves correspond to 100 and 500 mA drive currents, respectively.

power from -3.3 to $+3.3$ dB-m, both η and OSNR are reduced. This indicates that pump power should be optimized suitably. We turn to this issue next.

IV. OPTIMIZATION OF PUMP AND SIGNAL POWERS

In this section, we first investigate the role of input pump power P_0 by varying it in the range of -8 to $+8$ dB-m. This range corresponds to the range over which the net device gain was measured in Fig. 4(b), and over which the intraband FWM effects are negligible. The SOA current is fixed at 500 mA in the following measurements.

Fig. 8 shows the FWM spectra at three pump powers for (a) $\Delta\lambda = 0.5$ nm and (b) 2.5 nm. In both cases, peak heights at the signal and idler wavelengths decrease with increasing pump power, indicating that a higher pump power leads to smaller values of η . The reason for this behavior has been discussed in Section II in the context of Fig. 1(b) and is related to pump-induced gain saturation. As the pump is amplified inside the SOA, its power increases and can become comparable to the ASE power near the output SOA end. At a relatively low input pump power close to 0.1 mW, total ASE power dominates the pump power over nearly the entire SOA length. However, as input pump power exceeds 1 mW, gain saturation induced by an intense pump decreases the ASE power near the output SOA end, which increases the gain-recovery time and reduces the conversion efficiency. Clearly, high input pump powers should be avoided for wavelength converters based on SOAs making use of ASE-induced gain saturation.

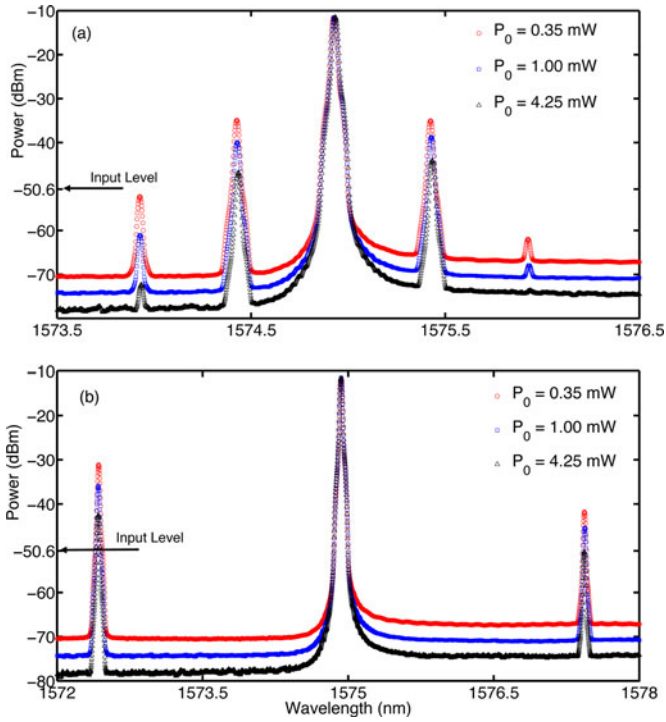


Fig. 8. FWM spectra observed at three input pump powers for pump-signal detunings of (a) 0.5 nm and (b) 2.5 nm. The SOA current is 500 mA and the signal level (-20.3 dB·m) is marked by an arrow.

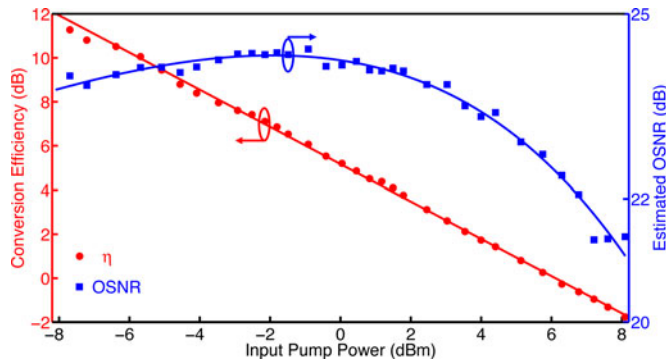


Fig. 9. Conversion efficiency (circles) and estimated OSNR (squares) measured as a function of P_0 at 500-mA drive current. Solid lines represent a fit to the experimental data. Input signal power was $10 \mu\text{W}$ at a pump-signal detuning of 2.5 nm.

However, we should pay attention to the OSNR before concluding that lower input pump powers are always better. We can see from Fig. 8 that both the in-band ASE spectral density and the peak heights at the idler wavelength are reduced with increasing P_0 . The qualitative behavior of OSNR with increasing pump powers cannot be inferred from this. Therefore, to clearly understand the tradeoff associated with increasing the input pump power, we show in Fig. 9, how η and OSNR evolve as a function of P_0 . We see clearly that, while η decreases monotonically with increasing P_0 , the OSNR exhibits a broad maximum near $P_0 = -2$ dB·m (about 0.6 mW). After this maximum, the OSNR drops when P_0 is increased beyond 2 dB·m. The reason is understood by noting that, beyond $P_0 = 2$ dB·m, reduction in the idler power becomes much more severe compared to reduction in the in-band noise. The optimum value of

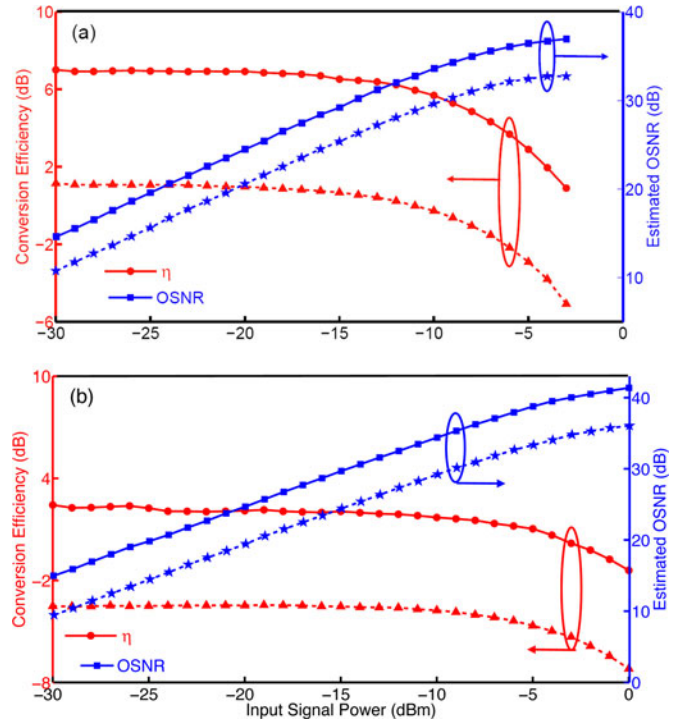


Fig. 10. Conversion efficiency and OSNR measured as a function of P_1 at (a) $P_0 = -2.2$ dB·m and (b) $P_0 = +3.3$ dB·m for $\Delta\lambda = 5$ nm. Dashed and solid lines correspond to drive currents of 300 and 500 mA, respectively.

P_0 for a wavelength converter is dictated to some extent by the design requirements. For example, if the requirement is that OSNR should exceed 23 dB, one can use pump powers as low as to 0.1 mW (-10 dB·m) to maximize η .

We should stress that the qualitative behavior of η and OSNR in Fig. 9 is quite different from that observed when intraband FWM is employed. In that case, it has been shown that both η and OSNR increase linearly with P_0 over a wide range of pump powers [15]–[17]. This feature can be attributed to the fact that gain saturation induced either by the pump or by the ASE plays little role in the intraband FWM process in traditional SOAs. Both η and OSNR therefore increase monotonically with increasing pump power because the idler power (governed mainly by the device gain) keeps increasing until the pump starts to reduce the device gain owing to the gain-compression effects [16].

We next consider the role of input signal power P_1 . Fig. 10 shows how η and OSNR vary as function of P_1 at two drive currents (300 and 500 mA) and at pump powers of (a) -2.2 dB·m and (b) $+3.3$ dB·m. The first thing to notice is that η remains almost constant until P_1 becomes comparable to P_0 and starts to saturate the SOA gain. In contrast, OSNR increases linearly with P_1 until it saturates to a value near 35 dB for large values of P_1 near 1 mW. These features can be understood as follows. As long as input signal power $P_1 \ll P_0$, the signal and the idler remain weak enough that they do not cause gain saturation, and η remains constant. The situation changes when P_1 becomes comparable to P_0 , and η begins to decrease with increasing P_1 . The OSNR improves with increasing P_1 because of an increase in the output idler power, while the ASE level remains nearly constant. The saturation of OSNR occurs once the idler gain

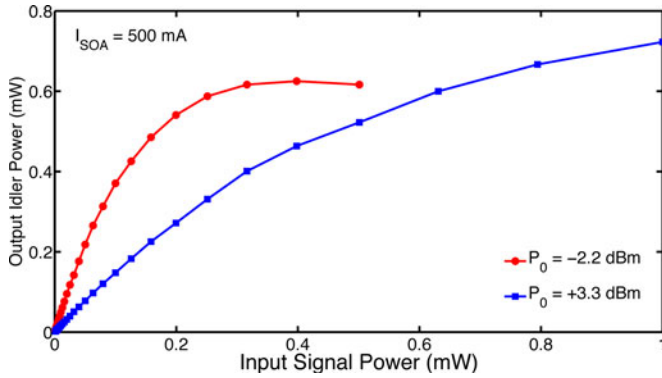


Fig. 11. Power transfer function for two pump powers at 500-mA SOA current. The wavelength shift is 5 nm.

is reduced because of gain saturation induced by the intense signal and idler fields. Practical wavelength converters based on SOAs typically require $\eta > -10$ dB and OSNR > 30 dB, while providing a wavelength shift of 10 nm or so [4], [21]. It can be seen from Fig. 10 that these conditions can be met for $P_1/P_0 \approx 0.1$. The performance of a wavelength converter can be characterized by its power transfer function showing output idler power as a function of input signal power. Fig. 11 shows this transfer function at two different input pump powers. A wavelength converter is usually operated in the linear regime of a power transfer function. Note that the linear regime of the transfer function extends over a wider range of signal powers for a higher input pump power. Although the dynamic range of signal powers is larger at higher pump powers, it comes at the expense of reduced conversion efficiency. Also, the nonlinear patterning effects due to slow SOA gain-recovery dynamics will come into play at higher pump and signal powers [21]. It is therefore likely that wavelength converters based on interband FWM will be operated at input pump powers close to 0.1 mW to take full advantage of ASE-induced ultrafast gain recovery. This will also ensure low energy consumption of such wavelength converters.

A wavelength converter can also act as an all-optical regenerator of a telecommunication channel if its power transfer function has a step-like shape that enables a reduction in signal noise at the converted wavelength [8], [43], [44]. As can be seen from Fig. 11, the shape of the power transfer function is far from being a step function. Although the plateau-like region at low pump powers may be useful for suppressing power fluctuations in the “1” bits, noise fluctuations in “0” bits cannot be suppressed.

V. VALIDITY OF THE THEORETICAL MODEL

In this section, we ask to what extent our experimental data are in agreement with the theoretical model of Section II. Our model predicts that relatively large wavelength shifts are possible in SOAs operated at high currents because enhanced ASE forced the carriers to recombine at a rate much faster than their natural recombination rate set by the carrier lifetime. This prediction indeed holds for our device. A more detailed comparison shows that our experiments are in agreement with the theoretical predictions qualitatively. A perfect quantitative agreement

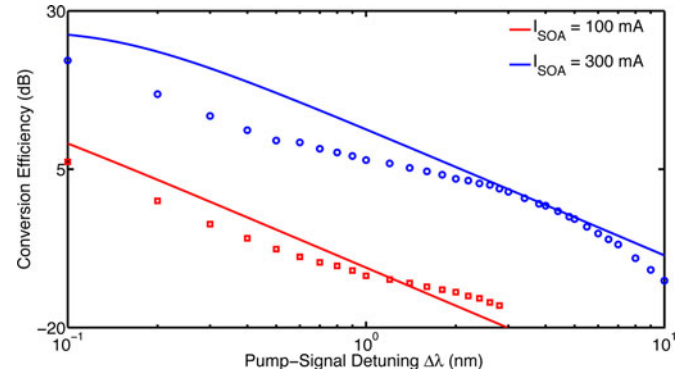


Fig. 12. Conversion efficiency as a function of $\Delta\lambda$ at SOA currents of 100 and 300 mA. Solid lines are obtained from our numerical model, whereas symbols represent experimental data. P_0 and P_1 are -3.3 and -20.3 dB-m, respectively.

TABLE II
CALCULATED AND OBSERVED VALUES OF $\Delta\lambda$ FOR $\eta = 1$ AND $P_0 = 0.47$ mW

SOA Current	Theory	Experiment
100 mA	0.24 nm	0.20 nm
300 mA	3.20 nm	3.6 nm
500 mA	7.14 nm	6.6 nm

is not expected because our theoretical model makes following three simplifying assumptions.

- 1) The effects of ASE are included by assuming that the average ASE power is constant along the SOA length and is related to the carrier density as $P_{\text{ASE}} = DN^2$ [34]. In reality, ASE power fluctuates in time and also varies along the amplifier length because of gain saturation induced by the amplified pump.
- 2) The SOA acts as a traveling-wave amplifier with no reflections at its two facets. In reality, there is always residual feedback at the facets, resulting in some Fabry–Perot effects that manifest as spectral fringes in the ASE spectra shown as the inset in Fig. 4(a). As seen there, the fringe amplitude becomes relatively large at 500-mA device current used for most of our measurements.
- 3) The third simplification consists of neglecting the wavelength dependence of the SOA gain over the wavelength range occupied by the pump, signal, and idler. This is a reasonable assumption for small pump–signal detunings ($\Delta\lambda < 5$ nm), given that the gain bandwidth of our SOA is close to 35 nm. However, this assumption is unlikely to hold for larger detunings.

As a check on the accuracy of our numerical predictions, we compare in Fig. 12 our theoretical predictions and experimental observations by plotting the conversion efficiency as a function of pump–signal detuning when the SOA is operated at 100- and 300-mA drive currents. The agreement is not expected to be perfect because our model completely ignores the Fabry–Perot effects resulting from the residual facet feedback. These effects become worse at higher drive currents, and our numerical model also becomes less accurate quantitatively. However, it still makes reasonable qualitative predictions. As an example, Table II compares the experimentally observed values with the

theoretically calculated pump–signal detunings for which we obtain 100% conversion efficiency (output idler power equals input signal power) in the case of 0.47-mW input pump power.

It is possible to improve the numerical model by including the ASE effects more accurately. One approach divides the ASE spectrum into multiple frequency bins and writes for each spectral slice of the ASE two equations corresponding to propagation in the forward and backward directions and solve them together the equations for the pump, signal, and idler fields. Up to 45 equations need to be solved simultaneously to accurately calculate the gain and the carrier density at each point of the amplifier [32]. The inclusion of facet reflections adds additional complexity as one has to consider the forward and backward propagation of the pump, signal, and idler fields as well. Even a small reflection due to residual facet reflectivity can be greatly amplified within the device, especially at high currents when the device gain is high.

VI. CONCLUDING REMARKS

In this paper, we have studied, both theoretically and experimentally, whether interband FWM can be used for wavelength conversion in SOAs driven at currents high enough that ASE itself begins to saturate the SOA gain. We used conversion efficiency and OSNR as two metrics to characterize the wavelength-conversion process. Across a broad range of wavelength shifts (as large as 20 nm), we observed an increase in the conversion efficiency of over 20 dB, and a corresponding increase in the OSNR of over 12 dB, as the SOA current was increased from 100 to 500 mA. Our experimental observations are in qualitative agreement with the theoretical predictions. As seen in Fig. 7(a), wavelength shifts ($2\Delta\lambda$) close to 15 nm are possible at high drive current levels that reduce the gain-recovery time to near 10 ps, while maintaining a high conversion efficiency ($\eta = 1$) and a high OSNR close to 25 dB. If we consider 10% conversion efficiency acceptable for a wavelength converter, wavelength shifts >25 nm are possible.

A major advantage of the ASE-enhanced interband FWM scheme is that input pump powers required for wavelength conversion are much lower ($P_0 < 0.5$ mW) than those employed in the case of intraband FWM. This feature reduces the electrical power consumption for such wavelength converters by more than a factor of 10. We discussed the issue of optimum pump power and found that high conversion efficiencies over a broad range of input signal powers are possible even at pump powers as low as 0.1 mW. However, the OSNR of the converted signal at such pump levels may be below 25 dB because input signal power in this case must be considerably less than 0.1 mW. If the design criterion requires an OSNR of 30 dB or more, input signal power should be close to 0.1 mW, and this requires an input pump power close to 1 mW.

A realistic wavelength converter for WDM systems must operate on pulsed signals at a bit rate of 10 Gb/s or more. We expect our conclusions based on CW experiments to hold for pulsed data channels, with minor modifications, as far as conversion efficiency and OSNR are concerned. In the case of ON–OFF keying, a partial recovery of the SOA gain during successive pulses will introduce nonlinear patterning effects. This problem

would be less severe for formats based on phase modulation (such as differential phase-shift keying). Another practical issue is related to the polarization dependence of FWM efficiency. This problem can be solved to a large extent if two orthogonally polarized pumps are employed. However, the performance of such a wavelength converter is likely to degrade if the total pump power increases considerably.

ACKNOWLEDGMENT

P. P. Baveja acknowledges the Swedish Institute Guest Scholarship.

REFERENCES

- [1] C. M. Gallep, H. J. S. Dorren, and O. Raz, “Four-wave-mixing-based dual-wavelength conversion in a semiconductor optical amplifier,” *IEEE Photon. Technol. Lett.*, vol. 22, no. 21, pp. 957–959, Nov. 2010.
- [2] P. Runge, C-A Bunge, and K. Petermann, “All-Optical wavelength conversion with extinction ratio improvement of 100 Gb/s RZ-signals in ultralong bulk semiconductor optical amplifiers,” *IEEE J. Quantum Electron.*, vol. 46, no. 6, pp. 937–944, Jun. 2010.
- [3] D. Nielsen and S. L. Chuang, “Four-wave mixing and wavelength conversion in quantum dots,” *Phys. Rev. B*, vol. 81, no. 3, pp. 035305-1–035305-11, Jan. 2010.
- [4] G. Contestabile, L. Banchi, M. Presi, and E. Ciaramella, “Investigation of transparency of FWM in SOAs to advanced modulation formats involving intensity, phase, and polarization multiplexing,” *J. Lightw. Technol.*, vol. 27, no. 19, pp. 4256–4261, Oct. 2009.
- [5] A. Capua, S. O’Duill, V. Mikhelashvili, G. Einstien, J. P. Reithmaier, A. Somers, and A. Forchel, “Cross talk free multi channel processing of 10 Gbit/s data via four wave mixing in a 1550 nm InAs/InP quantum dash amplifier,” *Opt. Exp.*, vol. 16, no. 23, pp. 19072–19077, Nov. 2008.
- [6] H. Simos, I. Stamatakis, and D. Syvridis, “Relative intensity noise performance of wavelength converters based on four-wave mixing in semiconductor optical amplifiers,” *IEEE J. Quantum Electron.*, vol. 43, no. 5, pp. 370–377, May 2007.
- [7] S. Radic, C. J. McKinstire, R. M. Jopson, J. C. Centanni, Q. Lin, and G. P. Agrawal, “Record performance of parametric amplifier constructed with highly nonlinear fiber,” *Electron. Lett.*, vol. 39, no. 11, pp. 838–839, May 2003.
- [8] S. Radic, C. J. McKinstire, R. M. Jopson, J. C. Centanni, and A. R. Chraplyvy, “All-optical regeneration in one- and two-pump parametric amplifiers using highly nonlinear optical fiber,” *IEEE Photon. Technol. Lett.*, vol. 15, no. 7, pp. 957–959, Jul. 2003.
- [9] M. Hirano, T. Nakanishi, T. Okuno, and M. Onishi, “Silica-based highly nonlinear fibers and their application,” *IEEE J. Sel. Topics Quantum Electron.*, vol. 15, no. 1, pp. 103–113, Jan./Feb. 2009.
- [10] G. P. Agrawal, “Population pulsations and nondegenerate four-wave mixing in semiconductor lasers and amplifiers,” *J. Opt. Soc. Amer. B*, vol. 5, no. 1, pp. 147–159, Jan. 1988.
- [11] M. P. Dlubek, S. N. Kaunga-Nyirenda, A. J. Phillips, S. Sujecki, I. Harrison, and E. C. Larkins, “Experimental verification of the existence of optically induced carrier pulsations in SOAs,” *Opt. Commun.*, vol. 283, no. 7, pp. 1481–1484, Apr. 2010.
- [12] G. P. Agrawal, “Highly nondegenerate four-wave mixing in semiconductor lasers due to spectral hole-burning,” *Appl. Phys. Lett.*, vol. 51, no. 5, pp. 302–304, 1987.
- [13] J. Zhou, N. Park, K. J. Vahala, M. A. Newkirk, and B. I. Miller, “Four-wave mixing wavelength conversion efficiency in semiconductor travelling-wave amplifier measured to 65 nm of wavelength shift,” *IEEE Photon. Technol. Lett.*, vol. 6, no. 8, pp. 984–987, Aug. 1994.
- [14] A. Mecozzi, S. Scotti, A. D’Ottavi, E. Iannone, and P. Spano, “Four-wave mixing in travelling-wave semiconductor amplifiers,” *IEEE J. Quantum Electron.*, vol. 31, no. 4, pp. 689–699, Apr. 1995.
- [15] A. D’Ottavi, E. Iannone, A. Mecozzi, S. Scotti, P. Spano, R. Dall’Ara, J. Eckner, and G. Guekos, “Efficiency and noise performance of wavelength converters based on FWM in semiconductor optical amplifiers,” *IEEE Photon. Technol. Lett.*, vol. 7, no. 4, pp. 357–359, Apr. 1995.
- [16] M. A. Summerfield and R. S. Tucker, “Noise figure and conversion efficiency of four-wave mixing in semiconductor optical amplifiers,” *Electron. Lett.*, vol. 31, no. 14, pp. 1159–1160, Jul. 1995.

- [17] M. A. Summerfield and R. S. Tucker, "Optimization of pump and signal powers for wavelength converters based on FWM in semiconductor optical amplifiers," *IEEE Photon. Technol. Lett.*, vol. 8, no. 10, pp. 1316–1318, Oct. 1996.
- [18] K. Obermann, I. Koltchanov, K. Petermann, S. Diez, R. Luwig, and H. G. Weber, "Noise analysis of frequency converters utilizing semiconductor-laser amplifier," *IEEE J. Quantum Electron.*, vol. 33, no. 1, pp. 81–88, Jan. 1997.
- [19] D. F. Geraghty, R. B. Lee, M. Verdiell, M. Ziari, and K. J. Vahala, "Wavelength conversion for WDM communication systems using four-wave mixing in semiconductor optical amplifiers," *IEEE J. Sel. Topics Quantum Electron.*, vol. 3, no. 5, pp. 1146–1155, Oct. 1997.
- [20] S. Diez, C. Schmidt, R. Ludwig, H. G. Weber, K. Obermann, S. Kindt, I. Koltchanov, and K. Petermann, "Four-wave mixing in semiconductor optical amplifiers for frequency conversion and fast optical switching," *IEEE J. Sel. Topics Quantum Electron.*, vol. 3, no. 5, pp. 1131–1145, Oct. 1997.
- [21] L. Lu, Y. Dong, H. Wang, W. Cai, and S. Xie, "Bit-error-rate performance dependence on pump and signal powers of wavelength converter based on FWM in semiconductor optical amplifiers," *IEEE Photon. Technol. Lett.*, vol. 12, no. 7, pp. 855–857, Jul. 2000.
- [22] Z. Li, Y. Dong, J. Mo, Y. Wang, and C. Lu, "Cascaded all-optical wavelength conversion for RZ-DPSK signal based on four-wave mixing in semiconductor optical amplifier," *IEEE Photon. Technol. Lett.*, vol. 16, no. 7, pp. 1685–1687, Jul. 2004.
- [23] S.-L. Lee, P.-M. Gong, and C.-T. Yang, "Performance enhancement on SOA-based four-wave-mixing wavelength conversion using an assisted beam," *IEEE Photon. Technol. Lett.*, vol. 14, no. 12, pp. 1713–1715, Dec. 2002.
- [24] D.-Z. Hsu, S.-L. Lee, P.-M. Gong, Y.-M. Lin, S. S. W. Lee, and M. C. Yuang, "High-efficiency wide-band SOA-based wavelength converters by using dual-pumped four-wave mixing and an assist beam," *IEEE Photon. Technol. Lett.*, vol. 16, no. 8, pp. 1903–1905, Aug. 2004.
- [25] J.-T. Hsieh, P.-M. Gong, S.-L. Lee, and J. Wu, "Improved dynamic characteristic on four-wave mixing wavelength conversion in light-holding SOAs," *IEEE J. Sel. Topics Quantum Electron.*, vol. 10, no. 5, pp. 1187–1196, Sep/Oct. 2004.
- [26] Y. Hong, P. S. Spencer, and K. A. Shore, "Wide-band polarization-free wavelength conversion based on four-wave mixing in semiconductor optical amplifier," *IEEE J. Quantum Electron.*, vol. 40, no. 2, pp. 152–156, Feb. 2004.
- [27] C. Politi, D. Klionidis, and M. J. O'Mahony, "Wavelength converters based on four-wave mixing in SOAs," *J. Lightw. Technol.*, vol. 24, no. 3, pp. 1203–1217, Mar. 2006.
- [28] G. Talli and M. J. Adams, "Gain recovery acceleration in semiconductor optical amplifiers employing a holding beam," *Opt. Commun.*, vol. 245, nos. 1–6, pp. 363–370, Jan. 2005.
- [29] F. Girardin, G. Guekos, and A. Houbavlis, "Gain recovery of bulk semiconductor optical amplifiers," *IEEE Photon. Technol. Lett.*, vol. 10, no. 6, pp. 784–786, Jun. 1998.
- [30] L. Zhang, I. Kang, A. Bhardwaj, N. Sauer, S. Cabot, J. Jaques, and D. T. Nielson, "Reduced recovery time semiconductor optical amplifiers using p-type-doped multiple quantum wells," *IEEE Photon. Technol. Lett.*, vol. 18, no. 22, pp. 2323–2325, Nov. 2006.
- [31] R. Giller, R.J. Manning, G. Talli, R. P. Webb, and M. J. Adams, "Analysis of the dimensional dependence of semiconductor optical amplifier recovery speeds," *Opt. Exp.*, vol. 15, no. 4, pp. 1773–1782, Feb. 2007.
- [32] A. M. de Melo and K. Petermann, "On the amplified emission noise modelling of semiconductor optical amplifiers," *Opt. Commun.*, vol. 281, no. 18, pp. 4598–4605, Sep. 2008.
- [33] A. Borghesani, "Semiconductor optical amplifiers for advanced optical applications," in *Proc. 8th Int. Conf. Transparent Opt. Netw.*, Nottingham, U.K., Jun. 18–22, 2006, pp. 119–122.
- [34] P. P. Baveja, D. N. Maywar, A. M. Kaplan, and G. P. Agrawal, "Self-phase modulation in semiconductor optical amplifiers: Impact of amplified spontaneous emission," *IEEE J. Quantum Electron.*, vol. 46, no. 9, pp. 1396–1403, Sep. 2010.
- [35] F. Girardin, J. Eckner, G. Guekos, R. Dall'Ara, A. Mecozzi, A. D'Ottavi, F. Martelli, S. Scotti, and P. Spano, "Low-noise and very high-efficiency four-wave mixing in 1.5-mm-long semiconductor optical amplifiers," *IEEE Photon. Technol. Lett.*, vol. 9, no. 6, pp. 746–748, Jun. 1997.
- [36] S. Jarabo and A. Tomás, "Experimental study on wave-mixing in semiconductor optical amplifiers," *Opt. Commun.*, vol. 281, no. 14, pp. 3872–3877, Jul. 2008.
- [37] G. P. Agrawal and N. K. Dutta, *Semiconductor Lasers*, 2nd ed. New York: Van Nostrand Reinhold, 1993.
- [38] X. Li, M. J. Adams, D. Alexandropoulos, and I. F. Lealman, "Gain recovery in semiconductor optical amplifiers," *Opt. Commun.*, vol. 281, no. 13, pp. 3466–3470, Jul. 2008.
- [39] S. Fu, W. Du, P. Shum, C. Wu, D. Hak, and L. Zhang, "Measurement of SOA linewidth enhancement factor with a Sagnac fiber loop," *IEEE Photon. Technol. Lett.*, vol. 18, no. 18, pp. 1934–1936, Sep. 2006.
- [40] J. Wang, A. Maitra, C. G. Poulton, W. Freude, and J. Leuthold, "Temporal dynamics of alpha factor in semiconductor optical amplifiers," *J. Lightw. Technol.*, vol. 25, no. 3, pp. 891–900, Mar. 2007.
- [41] X. Liu, Y.-H. Kao, S. Chandrasekhar, I. Kang, S. Cabot, and L. L. Buhl, "OSNR monitoring method for OOK and DPSK based on optical delay interferometer," *IEEE Photon. Technol. Lett.*, vol. 19, no. 15, pp. 1172–1174, Aug. 2007.
- [42] G. P. Agrawal, *Lightwave Technology: Components and Devices*. Hoboken, NJ: Wiley, 2004.
- [43] L. Provost, C. Finot, P. Petropoulos, T. Mukasa, and D. J. Richardson, "Design scaling rules for 2R-optical self-phase modulation based regenerators," *Opt. Exp.*, vol. 15, no. 8, pp. 5100–5113, Apr. 2007.
- [44] G. Gavioli, B. C. Thomsen, V. Mikhailov, and P. Bayvel, "Cascadability properties of optical 3r regenerators based on SOAs," *J. Lightw. Technol.*, vol. 25, no. 9, pp. 2766–2775, Sep. 2007.



Prashant P. Baveja (S'10) received the B.E. degree from the Delhi College of Engineering, University of Delhi, New Delhi, India, in 2006, where he was an Undergraduate Researcher at TIFAC CORE (Technology Information Forecasting and Assessment Council: Center of research and Excellence) labs. He is currently working toward the Ph.D. degree in optics at the Institute of Optics, University of Rochester, Rochester, NY.

His research interests include nonlinear optics in semiconductor optical amplifiers, thermal effects in vertical cavity surface emitting lasers, all-optical signal processing, nonlinear fiber optics, optical communication, and Raman amplification.

Mr. Baveja is a student member of the Optical Society of America.



Drew N. Maywar (S'97–M'06) received the B.S., M.S., and Ph.D. degrees in optical engineering from the Institute of Optics, University of Rochester, Rochester, NY, and B.A. degree in religion from the same university.

He was a Fulbright Scholar from 1993 to 1994 at Osaka University. Dr. Maywar was a member of Technical Staff at Bell Laboratories, Lucent Technologies from 2000 to 2003 and a Scientist at the University of Rochester from 2003 to 2009. In 2009, he joined the Electrical, Computer, and Telecommunications Engineering Technology Department, Rochester Institute of Technology, Rochester, NY, as an Assistant Professor. He is the coauthor of more than 35 papers and a book chapter. His research interests include all-optical signal processing, photonic memory, and fiber-optic communications.

Dr. Maywar is a member of the Optical Society of America. He was a recipient of Dissertation Enhancement Award in 1998 from National Science Foundation for research at the University of Tokyo.



Govind P. Agrawal (M'83–SM'86–F'96) received the B.Sc. degree from the University of Lucknow, Lucknow, Uttar Pradesh, India, in 1969, and the M.Sc. and Ph.D. degrees from the Indian Institute of Technology, New Delhi, India, in 1971 and 1974, respectively.

After holding positions at Ecole Polytechnique, France, City University of New York, and AT&T Bell Laboratories, he joined the Faculty of the Institute of Optics, University of Rochester, in 1989, where he is currently a Professor of Optics, a Professor of Physics, and a Senior Scientist at the Laboratory for Laser Energetics. He is the author or coauthor of eight books and 380 research papers in the field of lightwave technology.

Dr. Agrawal is a Fellow of the Optical Society of America. He is also a Life Fellow of the Optical Society of India.